The Journal of Physical Chemistry Letters

Surfaces, Interfaces, and Catalysis; Physical Properties of Nanomaterials and Materials

Acidity Constants of the Hematite-Liquid Water Interface from ab-initio Molecular Dynamics

Oliver R. Gittus, Guido F. von Rudorff, Kevin M. Rosso, and Jochen Blumberger

J. Phys. Chem. Lett., **Just Accepted Manuscript** • DOI: 10.1021/acs.jpclett.8b01870 • Publication Date (Web): 04 Sep 2018

Acidity Constants of the Hematite-Liquid Water Interface from *ab-initio* Molecular Dynamics

Oliver R. Gittus[a], Guido Falk von Rudorff[b], Kevin M. Rosso[c], and Jochen Blumberger[b*]
E-mail:
* to whom correspondence should be addressed:
e-mail: j.blumberger@ucl.ac.uk (J.B.)

[a] Department of Chemistry, University College London, London WC1E 6BT, UK.
[b] Department of Physics and Astronomy and Thomas Young Centre, University College London, London WC1E 6BT, UK.
[c] Physical Sciences Division, Pacific Northwest National Laboratory, Richland, Washington 99352, United States.

*To whom correspondence should be addressed

Abstract

The interface between transition metal oxides (TMO) and liquid water plays a crucial role in environmental chemistry, catalysis and energy science. Yet, the mechanism and energetics of chemical transformations at solvated TMO surfaces is often unclear, largely because of the difficulty to characterize the active surface species experimentally. The hematite (α-Fe_2O_3)-liquid water interface is a case in point. Here we demonstrate that *ab-initio* molecular dynamics is a viable tool for determining the protonation states of complex interfaces. The pK_a values of the oxygen-terminated (001) surface group of hematite, $\equiv$OH, and half-layer terminated (012) surface groups, $\equiv^2$OH and $\equiv^1OH_2$, are predicted to be (18.5 $\pm$ 0.3), (18.9 $\pm$ 0.6) and (10.3 $\pm$ 0.5) pK_a units, respectively. These are in good agreement with recent bond-valence theory based estimates, and suggest that the deprotonation of these surfaces require significantly more free energy input than previously thought.

Graphical TOC entry

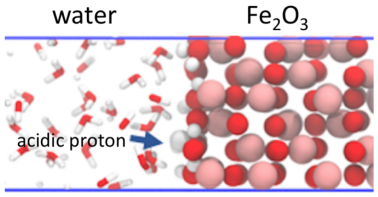

$$pK_a \approx \frac{1}{k_B T \ln 10} \int_0^1 d\eta \, \langle \Delta E \rangle_\eta$$

The hematite-liquid water interface (HLWI) plays an important role in many areas of the chemical sciences, especially in atmospheric colloid chemistry,[1] surface water and soil chemistry,[2] heterogeneous catalysis,[3] chemical energy storage[4] and energy harvesting,[5–9] to name a few. This is in part because hematite is abundant, cheap and stable in aqueous environments over a wide pH range. In particular, the potential use of hematite as photoanode material for photocatalytic water splitting has attracted much interest and motivated increasingly many studies of the HLWI.[10–12] Continuing efforts to improve the photocatalytic properties of hematite, for example via nanostructuring[13–15] and doping,[16] would benefit from a better knowledge of atomic-scale structure and interfacial processes.

For a better understanding of any interface, the interactions between solvent and solute are key. In the context of the HLWI, this includes the pH-dependent interactions between the surface and liquid water, with acid-base chemistry arising from the types and arrangement of Fe^{3+}-coordinating aquo/hydroxy groups. Solid surfaces can develop local charge imbalances that affect the apparent equilibrium constants of interfacial reactions; these electrostatic effects are highly variable with the pH and ionic strength of solution.[17] Intrinsic acidity constants correspond to the surface site in pure water divorced from these electrostatic effects. The intrinsic pK_a values of surface functional groups not only determine the protonation state of the system and the energetics of interfacial proton transfer reactions at a given pH, but also provide a link between experiment and theory. (With the caveat that intrinsic pK_a values cannot truly be accessed by experimental methods directly, without modeling assumptions about electrostatic factors arising from the composition and structure of the aqueous solution. Even second-harmonic generation spectroscopy techniques, which probe the surface potential, are calibrated based on double layer or constant capacitance models,[18,19] and in recent works[19] rely on additional modelling assumptions (Gouy-Chapman-Stern) to retrieve spatially resolved pK_a values.) Along with surface composition and electrical double layer structure, they also control surface speciation and the sorption of ions. Despite their significance, pK_a values of HLWI surface groups remain largely unclear: they are not known to within chemical accuracy, if at all.[20,21]

The modified[22–24] MUltiSIte Complexation (MUSIC) model[25,26] and the more recent model of Bickmore *et al.*[17,27] are two of the most successful empirical models for the pK_a prediction of surface functional groups. However, their respective estimates for HLWI surface groups differ by up to 10 pK_a units.[20,21] Indeed, there are multiple reasons to doubt whether existing bond-valence theory (BVT) based models can consistently predict accurate pK_a values for oxide surfaces; in the case of MUSIC: quantitative structure-activity relationships (QSARs) are calibrated based on the structures of (hydr)oxyacid monomers in solution; unrelaxed metal-oxygen bond lengths from bulk crystal structures are sometimes used, though surface relaxations are often non-negligible; the assignment of surface O^{2-} coordination numbers is ambiguous; and others (see ref. 28).[22,24,25,28] Furthermore, density functional theory-based molecular dynamics (DFT-MD) simulations indicate that H-bonding between hydr(oxo)-groups and water molecules adjusts to obey the valence sum rule, rather than maintaining a fixed valence based on O atom coordination, as predicted by MUSIC.[17] Bickmore *et al.*'s model predicts acidity constants based on three main factors: bond valence, metal-oxygen bond ionicity and molecular shape. Like MUSIC, it was calibrated using (hydr)oxyacid monomers, and is only applicable to surfaces if there are very localized electrostatic effects, such that the shape factor can be correctly predicted for surface functional groups.[17]

Surface relaxation and steric constraints of adsorbates near the surface are likely to have a strong impact on the accuracy of BVT models, since the bond valences are most sensitive to the bond distance parameter R_0.[24] This also highlights the importance of the reference data selection. While work based on crystal data has been successful in including hydrogen bond contributions,[22] this seems to come from limited variation of O···O distances in the test cases. Using O···O distances as a more resilient alternative has been suggested early[29] to deal with the high donor hydrogen bond sensitivity to minor geometry changes. Equally relevant to the source of the parametrization data is the functional shape.[30] Originally chosen over alternatives for convenience reasons[30] such that the second distance parameter B can be fixed to an effective value[29] and, hence, reporting R_0 is sufficient, investigating alternative descriptions might yield more accurate bond valences.

The BVT based models employ an empirical linear free energy relationship for the description of solvent effects on pK_a. Eliminating such a phenomenological relation requires either monitoring surface protonation as it evolves in MD simulations that allow for proton dissociation, or the application of free energy sampling methods.[31] The former approach has been applied to other iron oxide (magnetite[32] (Fe_3O_4) and goethite[33] (FeO(OH))) interfaces using classical force fields with dissociative water potentials. However, it is more difficult to model the HLWI using classical force fields; for example, even CLAYFF force fields specifically modified for hematite are unable to reproduce the atom number density profiles of surface protons from hybrid-DFT-MD simulations of the (001)-HLWI.[34–36] New force fields parameterized to reproduce the picosecond dynamics reported in hybrid-DFT-MD simulations[20,35,36] could be developed. Alternatively, MD simulations using reactive force fields fitted to other quantum-chemical data could be employed. ReaxFF[37,38] has proven successful in modeling surface-water interactions for other metal oxides.[39–45]

In this work we compute pK_a values for the hydroxy and aquo groups terminating the most prevalent surfaces of hematite: (001) and (012) in contact with liquid water. We adopt the thermodynamic integration scheme developed by Sprik and co-workers where both solute and solvent are treated at the DFT level.[46–48] This method has been successfully applied to several mineral-water interfaces,[31,49–52] but not to the HLWI, which is challenging to simulate due to the open-shell 3*d* orbital character underlying the antiferromagnetic spin pattern of hematite. We obtain pK_a values for the half-layer terminated (012) surface species directly from DFT-MD simulations at GGA+U level with dispersion corrections, that are in good agreement with the recent BVT estimates by McBriarty *et al.*[20] based on X-ray crystal truncation rod (CTR) diffraction data. Both our calculations and recent BVT estimates suggest that the deprotonation of these surfaces require significantly more free energy input than previously thought.[53]

In the following we briefly describe the thermodynamic integration method used to calculate the pK_a values, as well as the simulation details. The simulation results are then presented, and our DFT-MD pK_a values are compared to those previously reported in the literature. Finally, the results are analyzed and discussed in terms of the bonding and solvation structure of protonated

and deprotonated surface groups.

The aim is to compute the pK_a as

$$\mathrm{p}K_a = \frac{\Delta G^{\ominus}}{k_\mathrm{B} T \ln 10} \tag{1}$$

where $\Delta G^{\ominus}$ is the standard Gibbs free energy for acid-base dissociation:

$$\equiv \mathrm{AH}_{(s)} \rightarrow \equiv \mathrm{A}^-_{(s)} + \mathrm{H}^+_{(aq)} \tag{2}$$

where $\equiv$ denotes the surface. We note in passing that $\Delta G^{\ominus}$ includes all free enthalpy terms including the work term required to transfer the proton from the surface to bulk aqueous solution. In condensed phase reactions the difference between $\Delta G^{\ominus}$ and the standard reaction free energy $\Delta A^{\ominus}$ is negligibly small, hence $\Delta G^{\ominus} \approx \Delta A^{\ominus}$. $\Delta A^{\ominus}$ is made amenable to a combination of condensed phase DFT-MD and gas phase quantum chemistry calculations using the thermodynamic cycle shown in Figure 1.

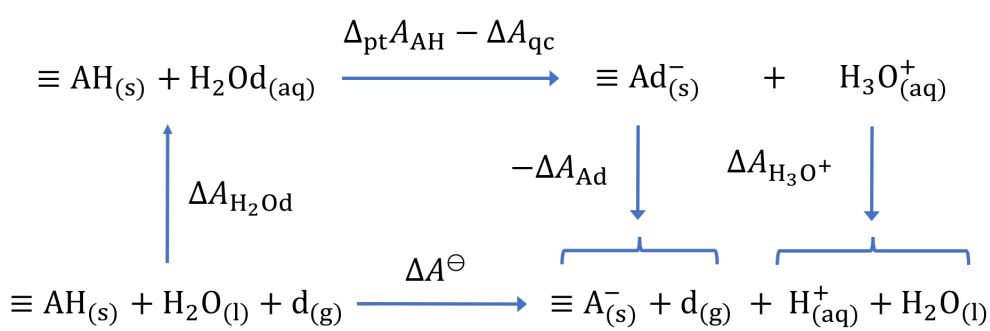

Figure 1: The thermodynamic cycle used to calculate the deprotonation free energy $\Delta A^{\ominus}$ and subsequently the pK_a via Eq. (1).

Starting with a water molecule in bulk water, a dummy proton d is connected to $\mathrm{H_2O}_{(l)}$ to form species $\mathrm{H_2Od}_{(aq)}$ at free energy cost $\Delta A_{\mathrm{H_2Od}}$. The dummy proton is connected to the oxygen atom by harmonic springs, such that the geometry of $\mathrm{H_2Od}$ resembles that of a hydronium ion. The dummy proton does not interact with the system otherwise. The proton transfer reaction is achieved at cost $\Delta_{pt}A_{AH}$ by simultaneously transforming the acidic proton of surface species $\equiv \mathrm{AH}_{(s)}$ into a

dummy proton, and the dummy proton connected to $H_2Od_{(aq)}$ into a proton. Finally, the dummy proton is detached from $\equiv Ad^-{}_{(s)}$ (free energy $-\Delta A_{Ad}$) and the hydronium ion is dissociated into a water molecule and a solvated proton (free energy $\Delta A_{H_3O^+}$). In the case where $\Delta_{pt}A_{AH}$ is calculated from a molecular dynamics simulation with classical nuclei, as is done here, a correction term $-\Delta A_{qc}$ must be added to account for quantum nuclear effects. The pK_a for Eq. (2) can then be written as:

$$pK_a = \frac{1}{k_B T \ln 10}\left(\Delta_{pt}A_{AH} - \Delta A_{qc} + \Delta A_{H_2Od} - \Delta A_{Ad} + \Delta A_{H_3O^+}\right) \tag{3}$$

We use a similar thermodynamic cycle as Mangold *et. al.*,[54] and readers are directed to this reference for further details on the free energy terms. The only difference is that we consider a proton transfer reaction instead of two deprotonation reactions. This is because a solid-liquid interface is a highly inhomogeneous system, and the alchemical transformation must be carried out in the same MD cell in order to maintain a constant electrostatic reference potential (i.e. the Poisson potential shift has no effect as the overall system conserves charge).[31,46,55]

The crucial step in the above thermodynamic cycle is the proton transfer reaction:

$$\equiv AH_{(s)} + H_2Od_{(aq)} \rightarrow \equiv Ad^-_{(s)} + H_3O^+_{(aq)}. \tag{4}$$

$\Delta_{pt}A_{AH}$ is calculated in the condensed phase using thermodynamic integration: separate DFT-MD simulations were carried out on the potential energy surfaces (PESs) defined by mapping potential

$$E_\eta = (1-\eta)E_0 + \eta E_1 \tag{5}$$

where $0 \leq \eta \leq 1$ is a coupling parameter. E_0 is the PES of solvated surface species $\equiv AH_{(s)}$ with $H_2Od_{(aq)}$ in bulk water (LHS of Eq. (4)), and E_1 is the PES of deprotonated surface species $\equiv Ad^-_{(s)}$

with $H_3O^+_{(aq)}$ in the solvent (RHS of Eq. (4)). Finally, thermodynamic integration yields:

$$\Delta_{\mathrm{pt}}A_{\mathrm{AH}} = \int_0^1 \langle \Delta E \rangle_\eta \, d\eta \tag{6}$$

$$\text{where,} \qquad \frac{\partial E_\eta}{\partial \eta} = E_1 - E_0 = \Delta E \tag{7}$$

In practice, few $\langle \Delta E \rangle_\eta$ points are available owing to the computational cost of DFT-MD. The five-point composite Simpson's rule (CSR) was used for integral evaluation:

$$\Delta_{\mathrm{pt}}A^{\mathrm{CSR}}_{\mathrm{AH}} = \frac{1}{12}(\langle \Delta E \rangle_0 + 4\langle \Delta E \rangle_{0.25} + 2\langle \Delta E \rangle_{0.5} + 4\langle \Delta E \rangle_{0.75} + \langle \Delta E \rangle_1) \tag{8}$$

In the linear response (LR) approximation, the integral is approximated by:

$$\Delta_{\mathrm{pt}}A^{\mathrm{LR}}_{\mathrm{AH}} = \frac{1}{2}(\langle \Delta E \rangle_0 + \langle \Delta E \rangle_1) \tag{9}$$

The LR approximation becomes exact if and only if the thermal probability distribution of ΔE is Gaussian. The additional free energy terms on the RHS of Eq. (3) are computed in the gas phase as described previously.[54]

The pK_a values of three functional groups were calculated: the $\equiv$OH group of the oxygen-terminated (001) surface, as well as the $\equiv^2$OH and $\equiv^1OH_2$ groups of the half-layer terminated (012) surface. The fully periodic simulated systems (Figure 2) comprised of a hematite slab protonated on both surfaces to yield a charge neutral interface, and solvated with a water layer large enough to exhibit bulk-like water between the solvation shells of the two surfaces.[36] The (001) system consisted of a $2 \times 2 \times 1$ hematite supercell built from hexagonal unit cells with an additional oxygen layer, and a $\sim$33 Å water layer (93 molecules). The (012) systems consisted of a $2 \times 1 \times 1$ hematite supercell built from the orthorhombic surface cell[21,56] commonly used for this interface, two terminating half-layers, and a $\sim$35 Å water layer (47 molecules). The modelled surfaces are charge neutral and correspond to hypothetical pH values that yield the point of zero net

proton charge (PZC). Not necessarily equivalent points of zero potential (PZPs) for these surfaces were measured at pH values 8-9, with $\mathrm{pH_{PZP}}(001) < \mathrm{pH_{PZP}}(012)$ (see ref. 57 for the relevant discussion).

Born-Oppenheimer DFT-MD simulations were carried using the open-source software package CP2K.[57,58] Simulations were performed in the NVT ensemble with a timestep of 0.5 fs. The PBE+U (U_{eff} = 4 eV on Fe 3d orbitals[12,59,60]) functional and atom-pairwise Grimme D3 dispersion correction[61] were used. m-TZVP and the short-range variants of m-DZVP basis functions of were used for H atoms and all other atoms respectively,[62] and the auxiliary plane wave basis cut-off was set to 400 Ry. Core electrons were represented by analytic Goedecker-Teter-Hutter pseudopotentials:[63–65] only the 3s, 3p, 3d and 4s electrons (for iron atoms) and the 2s and 2p electrons (for oxygen atoms) were treated explicitly. The simulation temperature was set to 330 K in order to compensate for the over-structuring and low self-diffusion constant of PBE water, which persists even with the D3 dispersion correction. Running the dynamics at the elevated temperature gives a better approximation to the experimental dynamics at room temperature.[66] For calculation of the pKa values according to Eq. (3) $T = 298$ K was used. Where applicable, equilibration times were determined using reverse cumulative averaging,[67] and ranged from 1-4 ps. This was followed by production runs of 8-12 ps for the (001) system and 15-38 ps for the (012) systems. Gas phase calculations for the free energy correction terms used the same functional and basis.

The harmonic potentials used to restrain the dummy proton take the from

$$V_r = \sum_{\text{bonds}} \frac{k_r}{2}(r - r_{\text{eq}})^2 + \sum_{\text{angles}} \frac{k_\theta}{2}(\theta - \theta_{\text{eq}})^2 \tag{10}$$

where parameters k_r, r_{eq}, k_θ and θ_{eq} were chosen to mimic the equilibrium geometry of the solvated species $\equiv\mathrm{AH}_{(s)}$ and $\mathrm{H_3O^+_{(aq)}}$, and are shown in Table 1. We note that the angle restraints for $\equiv$OH (001) biased sampling in favor of the out-of-plane configuration.[35] However, no significant difference in $\langle \Delta E \rangle_\eta$, and hence deprotonation free energy, was observed for the in-plane and out-of-plane configurations.

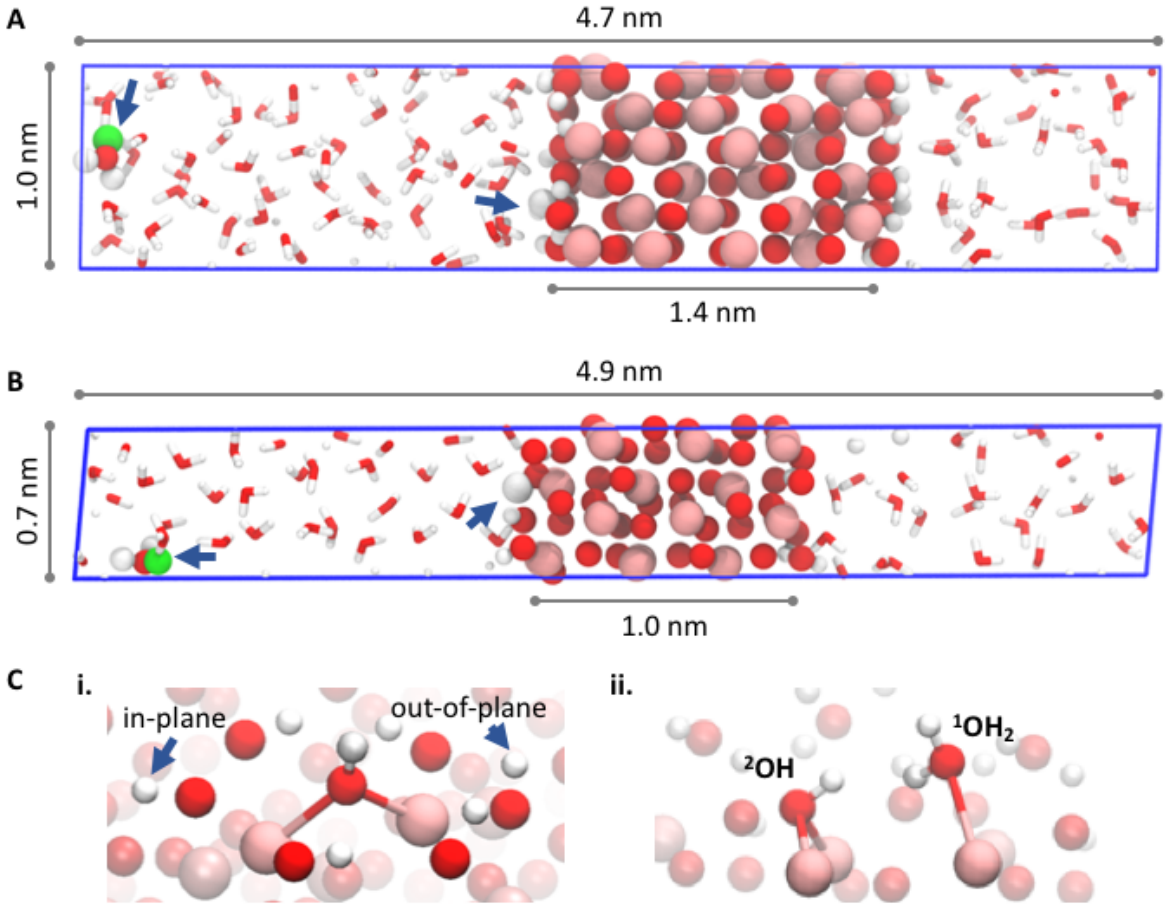

Figure 2: The simulated molecular dynamics systems and pictorial representation of the alchemical transformation used to compute the acidity constants of surface groups at the hematite-liquid water interface. Snapshots of the oxygen-terminated (001) (A) and half-layer-terminated (012) (B) interface systems. Fe, O and H atoms are shown in ochre, red and white respectively. Snapshots are taken from the E_0 trajectories: the dummy proton (in H_2Od) is shown in green, while the surface proton in question is depicted by an enlarged sphere, both are indicated to by arrows. Panel B shows the $\equiv{}^2OH$ (012) group. Panel C shows the bonding of the surface groups: (i.) the $\equiv OH$ (001) group and its six neighboring hydroxy groups, with in-plane and out-of-plane proton configurations highlighted by arrows; (ii.) the $\equiv{}^2OH$ and $\equiv{}^1OH_2$ (012) groups.

Table 1: Force constants and equilibrium values for bonds (k_r, r_{eq}) and angles (k_θ, θ_{eq}) of the restraining potential V_r for the dummy proton (Eq. (10)).

Species	Bond	k_r [a.u.]	r_{eq} [Å]	Angle	k_θ [a.u.]	θ_{eq} [deg.]
$\equiv$Od$^-$ (001)	O-d	0.2	1.00	O-O-d[a]	0.001	90
$\equiv$^{2}Od$^-$ (012)	O-d	0.2	1.00	O-O-d[b]	0.025	133
$\equiv$^{1}OHd$^-$ (012)	O-d	0.2	1.00	H-O-d	0.117	109
				Fe-O-d	0.066	101
H_2Od[c]	O-d	0.2	1.00	H-O-d	0.2	111

[a] 6 angle restraints were applied. [b] Includes the O bonded to d and its crystallographic image inside bulk hematite; the O-O displacement vector approximates the surface normal. [c] Parameters taken from ref. 46 and 54.

Table 2: Local normal mode frequencies of the dummy proton d ($\nu_{Ad,i}$) and quantum mechanically treated proton ($\nu_{AH,i}$) for the surface groups of hematite in vacuum, $\equiv$Ad$^-$ and $\equiv$AH respectively. Frequencies and moments of inertia[a] (I) for gas phase water/hydronium are also given, as required for the free energy correction terms.

Species	$\nu_{Ad,i}$ [cm^{-1}]	$\nu_{AH,i}$ [cm^{-1}]	I [a.u.]
$\equiv$OH (001)	170, 170, 2290	780, 920, 3090	
$\equiv$^{2}OH (012)	10, 430, 2290	570, 810, 3580	
$\equiv$^{1}OH$_2$ (012)	330, 1110, 2290	780, 1240, 3130	
H_2O		1610, 3710, 3820	4180, 7640, 11820
H_3O^+	1320, 1890, 1970, 2370, 3710, 3820	900, 1640, 1660, 3440, 3540, 3570	9880, 10590, 17060

[a] For H_2O and H_2Od only, as required for the calculation of ΔA_{H_2Od} (see ref. 46).

Our pK_a estimates are given in Table 3 and their corresponding thermodynamic integrals are shown in Figure 3. As has been previously established,[46,54] the LR approximation is largely inadequate: deviations from the CSR range from 2.6-3.3 pK_a units.

Table 3: The thermodynamic integrals, thermochemical corrections and intrinsic pK_a values for the surface functional groups. pK_a values correspond to a temperature of 298 K.

Species	ΔA_{pt}[a][eV]		Thermochemical Corrections [eV]			pK_a	
	LR[b]	CSR[c]	$\Delta\Delta A_{Ad}$[d]	ΔA_{qc}[e]	$\Delta A_{H_3O^+}$[f]	LR[b]	CSR[c]
$\equiv$OH (001)	1.36 ± 0.04	1.17 ± 0.02	0.08	-0.03		21.7 ± 0.7	18.5 ± 0.3
$\equiv^2$OH (012)	1.00 ± 0.05	1.16 ± 0.03	0.14	-0.02	-0.19	16.2 ± 0.8	18.9 ± 0.6
$\equiv^1OH_2$ (012)	0.59 ± 0.06	0.77 ± 0.03	0.02	-0.02		7 ± 1	10.3 ± 0.5

[a]Free energy for the proton transfer reaction shown in Eq. (4); Using the [b]linear response approximation (Eq. (9)) and [c]composite Simpson's rule (Eq. (8)) to evaluate ΔA_{pt}; Overall free energy corrections (Figure 1) for [d]dummy atom insertion $\Delta\Delta A_{Ad} = \Delta A_{H_2Od} - \Delta A_{Ad}$, [e]quantum nuclear effects and [f] reaction $H_3O^+_{(aq)} \rightarrow H_2O_{(l)} + H^+_{(aq)}$.

At (18.5 $\pm$ 0.3), our DFT-MD pK_a estimate for the $\equiv$OH group of the oxygen-terminated (001)-HLWI is higher than previously predicted. Using a MUSIC model parameterized with bulk crystal structure data, the pK_a value of this surface group was first estimated at 11.9.[23] Subsequent MUSIC predictions using CTR data[69] of the interface provided a more accurate estimate of 12.4 pK_a units.[70] Lützenkirchen *et. al.* observed that upon aging, the surface potential vs. pH curve of the (001)-HLWI evolved to resemble the curve expected from MUSIC for the ideal oxygen-terminated surface (as opposed to the bi-domain surface structure, in which iron- and oxygen-terminations co-exist). Fitting this data using a purely diffuse layer model gave a pK_a of 13.7.[70] Similarly, using potentiometric titration data, a superposition of two triple layer models and an internally consistent fitting scheme, Chatman *et. al.* generated a pK_a value of 12.6 for the doubly coordinated hydroxy groups (Fe_2-OH) of the (001)-HLWI.[71] These empirical estimates rely on surface complexation models. As discussed in the following paragraph, other more recent BVT based models[17] have predicted substantially higher pK_a values for the Fe_2-OH groups of the (012)-HLWI.

The pK_a estimates for the half-layer terminated (012) surface groups also are higher than those

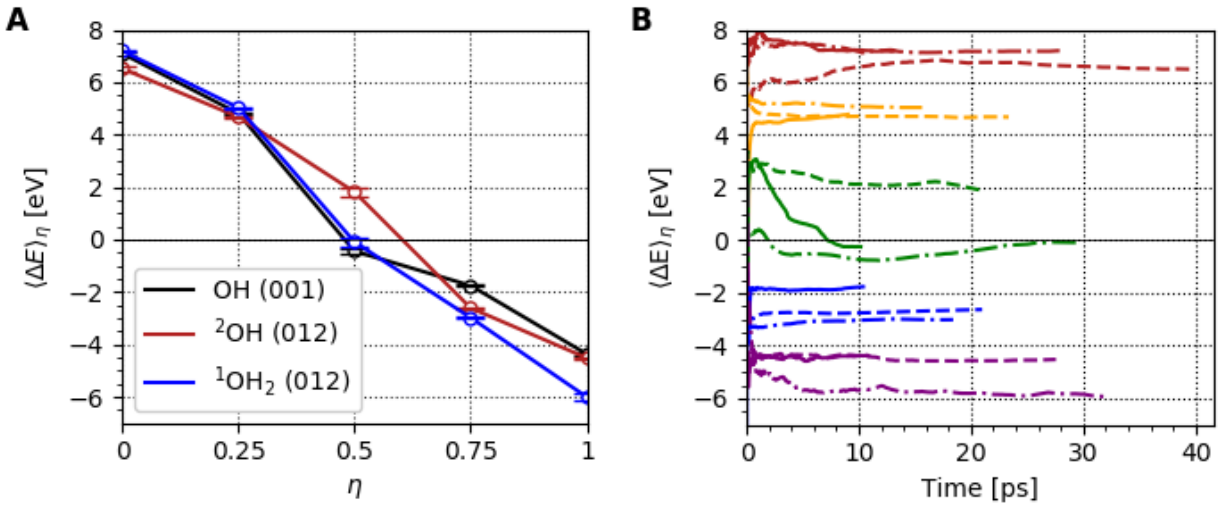

Figure 3: (A) The thermal average of the vertical energy gaps versus coupling parameter η for terminal oxygen species at the hematite-liquid water interface, as obtained from DFT-MD simulations. Error bars were obtained by block averaging.[68] The area below the (interpolated) data points corresponds to the free energy for proton transfer (Eq. (4)), approximating thermodynamic integral (Eq. (6)) using the composite Simpson's rule (Eq. (8)). (B) The running average of the vertical energy gaps. The average includes equilibration; final values may differ from those shown in A. $\equiv$OH (001), $\equiv^2$OH (012), and $\equiv^1$OH$_2$ (012) species are denoted by solid (-), dashed (---) and dot-dashed (-·-·) lines respectively. $\eta = 0, 0.25, 0.5, 0.75$ and 1 are shown in red, orange, green, blue and purple respectively.

previously reported. Tanwar *et. al.* predicted values of 2.0 for $\equiv^1OH_2$, and 7.9 for $\equiv^2OH$.[21] They calculated a static hydration and protonation model using DFT, and analyzed it using Hiemstra *et. al.*'s version[22] of MUSIC. More recent CTR experiments by McBriarty *et. al.* have yielded similar bond-valence sums for ^1O and ^2O, but significantly different pK_a values of (7.6 ± 0.9) and (17.5 ± 0.9) using Bickmore *et. al.*'s method.[20] Applying this method to Tanwar *et. al.*'s measured interface structure gave 10.9 and 12.4 pK_a units for $\equiv^1OH_2$ and $\equiv^2OH$ respectively:[20] estimates vary significantly between CTR experiments, even when the same QSAR model is used. Both QSARs calculate Fe-O bond-valence sums using the parameters of Brown and Altermatt ($R_0 = 1.759$ Å, $B = 0.37$ Å);[29] Tanwar *et. al.*'s MUSIC model additionally calculated O-H bond valence contributions using the method of Bargar *et. al.*[72]) However, Tanwar *et. al.*'s interfacial structure reports O-O separations between adsorbed water and surface groups as short as (2.0 ± 0.3) Å. As pointed out in a subsequent publication, this is perhaps unphysically short considering steric factors.[73] McBriarty *et. al.*'s estimates are therefore the most valid available for comparison. Given the associated uncertainties, their value for the $\equiv^2OH$ group agrees well with our value of (18.9 ± 0.6). A somewhat higher deviation is observed for the $\equiv^1OH_2$ group: our value of (10.3 ± 0.5) is ∼3 pK_a units higher.

The aforementioned BVT-based pK_a estimates input structural data from CTR diffraction experiments. CTR is not generally able to detect individual hydrogen atoms due to their small scattering cross-section. Consequently, the analysis of surface protonation environments and the exact nature of H-bonding in interfacial water is ambiguous when based on CTR data alone. Simulations constrained by experimental data have provided some insight; results can quantify H-bonding interactions, which are then used within refined MUSIC models. Machesky and coworkers have obtained bond valences from DFT geometry optimizations, and both classical and DFT-based MD simulations.[74–76] These simulations and resulting MUSIC models were constrained using potentiometric titration data, single-surface pH_{PZC} determination and CTR data. Studies of the (110) surface of rutile[74] (TiO_2) and cassiterite[75,76] (SnO_2) reproduced the pH_{PZC} values within ∼1.4 units, which is reasonable considering all the potential sources of error.[28] However, site-specific

pK_a values are expected to be less accurate: these predictions have differed significantly from DFT-MD based estimates for rutile.[31] pH_{PZC} values were derived from site-specific pK_a values averaged over the entire structure; this version of MUSIC may correctly predict average behavior, but not the acidity of individual functional groups. All BVT-based acidity QSARs are related exclusively to the conjugate base,[28] yet CTR gives time-averaged structural data. These models therefore assume that the structures of metal-oxygen surface groups are not affected by (de)protonation. As demonstrated by the average Fe-O bond lengths in Table 4, the structural response of surface groups to (de)protonation can be relatively large.

There are five main sources of error associated with the pK_a estimates presented in this work: finite MD sampling; thermodynamic integral evaluation, including the chosen numerical method and the number of E_η windows used; the accuracy of the PBE+U functional; finite size effects; and the assumptions[54] made in deriving the thermochemical corrections. The first is reflected in the statistical uncertainty, while the others cannot be readily quantified without appropriate benchmarks. Finite size effects were more significant in the (012) systems, for which the lateral dimensions of the simulation cells are comparable to that of the Eigen cation ($H_9O_4^+$). However, the smaller system sizes facilitated the longer trajectories (Figure 3B) required to adequately sample the more dynamic[20] interface. The employed DFT-MD-based method has been able to reproduce the pK_a values of small organic and inorganic acids within 1-2 units, even at GGA level.[48] Using three E_η windows, its application to amino acids gave an unsigned mean error of 2.1 pK_a units.[54] While caution must be exercised when comparing such different systems, these errors provide an indication of the level of accuracy expected from our pK_a estimates.

All three surface oxo groups are stabilized by stronger Fe-O bonds, as expected from electrostatic considerations. Upon deprotonation, a 0.37 Å decrease in Fe-O bond length was observed for $\equiv{}^1OH_2$ (012). Smaller average decreases were observed for the hydroxy groups, since they are stabilized by two bonds: the shorter (longer) Fe-O bond length decreased by 0.12 Å (0.21 Å) for $\equiv$OH (001), and by 0.20 Å (0.22 Å) for $\equiv{}^2$OH (012).

Contributions to the coordination number (CN) of the (de)protonated acidic sites are shown in

Table 4: The Fe-O bond lengths ($r_{\text{Fe-O}}$), coordination number[a] contributions from surface protons (CN_{surf}) and solvent molecules (CN_{solv}), and the total coordination number (CN_{total}), for the protonated and deprotonated acidic sites of hematite.

Species	Protonated				Deprotonated			
	$r_{\text{Fe-O}}$ [Å]	CN_{surf}	CN_{solv}	CN_{total}	$r_{\text{Fe-O}}$ [Å]	CN_{surf}	CN_{solv}	CN_{total}
$\equiv$OH (001)	1.95, 2.15	0.1	0.8	0.9	1.83, 1.94	0.6	1.0	1.6
$\equiv^2$OH (012)	2.05, 2.10	1.0	0.0	1.0	1.85, 1.89	1.0	0.9	1.9
$\equiv^1$OH$_2$ (012)	2.23	1.2	0.0	1.2	1.91	1.3	0.4	1.7

[a]Only H atoms within 2.4 Å of the $\equiv$O/$\equiv$O$^-$ species were counted. For the (012) surface, terminal aquo (surface) groups were distinguished from (solvent) water molecules using a Fe-OH$_2$ distance criteria of 3.0 Å - this corresponds to the first minimum in the Fe-OH$_2$ density profile (Figure 4B).

Table 4 and Figure 4. The CNs for the protonated and deprotonated $\equiv$OH (001) groups are 0.9 and 1.6 respectively. The $\equiv$O$^-$ (001) anion is stabilized by the both surface and solvent H atoms. As previously reported in hybrid-DFT-MD simulations,[35,36] we observe surface protons that point either parallel (in-plane) or perpendicular (out-of-plane) to the surface (Figure 2C(i.)). Approximately 80% of the 0.5 increase in CN from surface protons arose from in-plane protons. However, longer MD trajectories are required for a representative average over surface proton configurations. While deprotonation results in an increase of only 0.2 for the solvent contribution, the neighboring water molecule participates in a strong H-bond, with an average O-O distance of 2.5 Å. Indeed, the transition state for protonation was frequently observed: 48% of the sampled distances between the $\equiv$O$^-$ H-bond acceptor and the donated hydrogen were below 1.5 Å. While the entire proton transfer reaction did not occur during the simulation, it is expected to at longer timescales. Therefore in our simulations the deprotonated state is kinetically, not thermodynamically stable. The employed DFT-MD method enables us to estimate the pK_a values of species that are higher than that of liquid water (pK_a = 14.0), and therefore typically inaccessible to experimental measurements.

As previously reported in hybrid-DFT-MD simulations of the (012)-HLWI,[20] we observe the picosecond exchange of terminal aquo groups and adsorbed water molecules. The two species are distinguished by a Fe-OH$_2$ distance criterion of 3.0 Å - this corresponds to the first minimum in the Fe-OH$_2$ density profile (Figure 4B). The surface CN contributions for both $\equiv^2$OH and

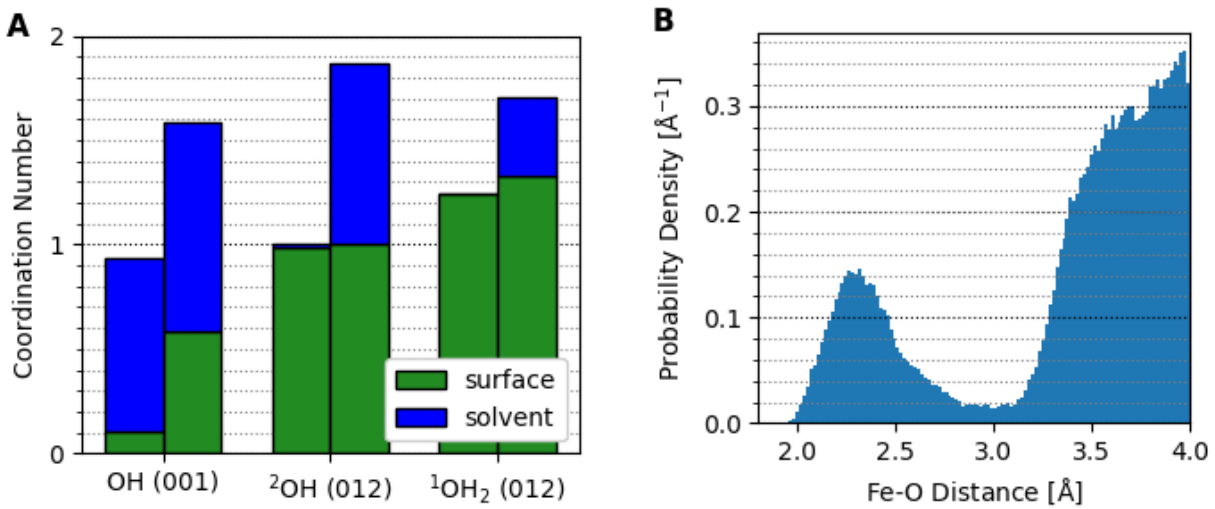

Figure 4: (A) Coordination numbers of the protonated (left) and deprotonated (right) acidic sites of hematite. Only H atoms within 2.4 Å of the $\equiv$O/$\equiv$O$^-$ species were counted. For the (012) surface, terminal aquo (surface) groups were distinguished from (solvent) water molecules using a Fe-OH$_2$ distance criteria of 3.0 Å. This corresponds to the first minimum in the Fe-OH$_2$ density profile for the (012) surface (B).

$\equiv^2$O$^-$ species arise exclusively from the nearest neighbouring terminal aquo group, which donates an H-bond of approximately equal strength (O-O distance of 2.6 Å) to $\equiv^2$OH/$\equiv^2$O$^-$. In the deprotonated case, the solvent contribution CN$_{solv}$ arises entirely from a neighbouring aquo group that detaches from the surface (and is thus redefined as a solvent water molecule); in order to donate a H-bond, this species must leave a Fe^{3+} site uncoordinated. However, the O-H bonds of neighbouring aquo groups were restrained to prevent the protonation of $\equiv^2$O$^-$. The observed $\equiv^2$O$^-$ solvent configuration therefore corresponds to a short-lived proton configuration.

The $\equiv^1$OH$^-$ (012) group is predominately stabilized by solvent water molecules, but also by $\equiv^2$OH groups. Both $\equiv^1$OH$_2$ and $\equiv^1$OH$^-$ accept an H-bond from the closest aquo group that contributes 1.0 to CN$_{surf}$; upon deprotonation, the average $\equiv^1$O-OH$_2$ distance remains approximately constant at 2.6 Å. The 0.1 increase in CN$_{surf}$ arises from the increased coordination by $\equiv^2$OH groups. As for the solvent contribution: when H-bonding with overlying water molecules (not those participating in ligand exchange), $\equiv^1$OH$_2$ acts only as the donor (no CN contribution), while $\equiv^1$OH$^-$ acts as both a donor and acceptor (CN contribution of 0.4). The accepted H-bonds

are approximately equal in strength to those in liquid water, with an average O-O distance of 2.8 Å. The coordination numbers CN, CN_{surf} and CN_{solv} were calculated from averages over the single (de)protonated species only; other $\equiv{}^{1}OH_2$ groups were observed to participate in H-bonding networks in which they accept H-bonds from solvent water molecules. More extensive sampling may shift the balance of CN_{surf} and CN_{solv}, while the total CN value is likely better converged.

In conclusion, we have used the DFT-MD-based thermodynamic integration to compute the intrinsic pK_a values of HLWI surface groups. These are the most accurate computational estimates to date. In line with recent BVT-based estimates,[20] our estimates suggest that protons at the HLWI may be less reactive than previously thought. Upon deprotonation, all three resultant bridging or terminal oxo groups are stabilized by stronger Fe-O bonds and H-bonds donated by overlying water molecules. Additionally, the $\equiv O^-$ (001) species is stabilized by an increased coordination by surface protons.

The next step in achieving a more comprehensive understanding of acidity and reactivity at the HLWI would be experimental confirmation. Scanning force microscopy (SFM) based methods[77] could offer accurate isoelectric point pH values of specific crystal faces. These, in turn, could be used to test various QSARs, and ultimately improve BVT-based pK_a estimates.[77] With further development, SFM measurements could in theory be extended to the single-site scale, where pK_a values could be extracted from force-pH curves. Sum-frequency vibrational spectroscopy probes the vibrational modes at the surface of specific crystal faces; analysis of the OH stretch region gives detailed microscopic structural information on surface protonation environments and H-bonding networks.[78,79] It has been applied to other mineral-water interfaces,[78,79] and in certain situations offers a possible route to information useful for constraining experimental pK_a values.

There is also cause for further computational work applying the same methodology reported herein to other HLWI surface groups. Unlike on the oxygen-terminated surface, $\equiv O^-$ and $\equiv OH_2^+$ groups coexist on the iron-terminated (001) surface in addition to neutral $\equiv OH$ groups. The pK_a values of these $\equiv OH$ and $\equiv OH_2^+$ groups are therefore necessary for a complete picture of acidity at the (001)-HLWI. However, PBE+U DFT-MD simulations are unable to reproduce a stable

iron-terminated (001)-HLWI, and more computationally demanding hybrid functionals would be required.[36] The strongly non-linear hysteretic pH-potential relationships observed in potentiometric pH titrations of specific hematite crystal faces is thought to stem from a “leaky screen" trapping mechanism.[80] This hypothesis could be (in)validated by calculating the pK_a of the $\equiv^3$OH (012) group when neighbouring ^{2}O species are singly protonated. Simulations to this end are currently underway in our laboratory.

Acknowledgement

GvR gratefully acknowledges a Ph.D. studentship co-sponsored by University College London and the Pacific Northwest National Laboratory through its Geosciences program supported by the U.S. Department of Energy’s Office of Science, Office of Basic Energy Sciences, within its Chemical Sciences, Geosciences and Biosciences Division.

Via our membership of the UK’s HEC Materials Chemistry Consortium, which is funded by EPSRC (EP/L000202), this work used the ARCHER UK National Supercomputing Service (http://www.archer.ac.uk). We are grateful to the UK Materials and Molecular Modelling Hub for computational resources, which is partially funded by EPSRC (EP/P020194/1).

References

(1) Ravishankara, A. R.; Rudich, Y.; Wuebbles, D. J. Physical Chemistry of Climate Metrics. *Chem. Rev.* **2015**, *115*, 3682–3703.

(2) Philippe, A.; Schaumann, G. E. Interactions of Dissolved Organic Matter with Natural and Engineered Inorganic Colloids: A Review. *Environ. Sci. Technol.* **2014**, *48*, 8946–8962.

(3) Kuhlenbeck, H.; Shaikhutdinov, S.; Freund, H.-J. Well-Ordered Transition Metal Oxide Layers in Model Catalysis – A Series of Case Studies. *Chem. Rev.* **2013**, *113*, 3986–4034.

(4) Reddy, M. V.; Subba Rao, G. V.; Chowdari, B. V. R. Metal Oxides and Oxysalts as Anode Materials for Li Ion Batteries. *Chem. Rev.* **2013**, *113*, 5364–5457.

(5) Sivula, K.; Le Formal, F.; Grätzel, M. Solar Water Splitting: Progress Using Hematite (α-Fe_2O_3) Photoelectrodes. *ChemSusChem* **2011**, *4*, 432–449.

(6) Lützenkirchen, J.; Heberling, F.; Supljika, F.; Preocanin, T.; Kallay, N.; Johann, F.; Weisser, L.; Eng, P. J. Structure–charge relationship – the case of hematite (001). *Faraday Discuss.* **2015**, *180*, 55–79.

(7) Shen, S. Toward efficient solar water splitting over hematite photoelectrodes. *J. Mater. Res.* **2014**, *29*, 29–46.

(8) Shen, S.; Lindley, S. A.; Chen, X.; Zhang, J. Z. Hematite heterostructures for photoelectrochemical water splitting: rational materials design and charge carrier dynamics. *Energy Environ. Sci.* **2016**, *9*, 2744–2775.

(9) Tamirat, A. G.; Rick, J.; Dubale, A. A.; Su, W.-N.; Hwang, B.-J. Using hematite for photoelectrochemical water splitting: a review of current progress and challenges. *Nanoscale Horiz.* **2016**, *1*, 243–267.

(10) Zhang, X.; Bieberle-Hütter, A. Modeling and Simulations in Photoelectrochemical Water Oxidation: From Single Level to Multiscale Modeling. *ChemSusChem* **2016**, *9*, 1223–1242.

(11) Nguyen, M.-T.; Seriani, N.; Piccinin, S.; Gebauer, R. Photo-driven oxidation of water on α-Fe_2O_3 surfaces: An ab initio study. *J. Chem. Phys.* **2014**, *140*, 064703.

(12) Nguyen, M.-T.; Seriani, N.; Gebauer, R. Water adsorption and dissociation on α-Fe_2O_3 (0001): PBE+U calculations. *J. Chem. Phys.* **2013**, *138*, 194709.

(13) Cesar, I.; Sivula, K.; Kay, A.; Zboril, R.; Grätzel, M. Influence of Feature Size, Film Thickness, and Silicon Doping on the Performance of Nanostructured Hematite Photoanodes for Solar Water Splitting. *J. Phys. Chem. C* **2009**, *113*, 772–782.

(14) Ling, Y.; Wang, G.; Wheeler, D. A.; Zhang, J. Z.; Li, Y. Sn-Doped Hematite Nanostructures for Photoelectrochemical Water Splitting. *Nano Lett.* **2011**, *11*, 2119–2125.

(15) Tsege, E. L.; Atabaev, T. S.; Hossain, M. A.; Lee, D.; Kim, H.-K.; Hwang, Y.-H. Cu-doped flower-like hematite nanostructures for efficient water splitting applications. *J. Phys. Chem. Solids* **2016**, *98*, 283–289.

(16) Zhou, Z.; Huo, P.; Guo, L.; Prezhdo, O. V. Understanding Hematite Doping with Group IV Elements: A DFT+ U Study. *J. Phys. Chem. C* **2015**, *119*, 26303–26310.

(17) Bickmore, B. R.; Rosso, K. M.; Tadanier, C. J.; Bylaska, E. J.; Doud, D. Bond-valence methods for pK_a prediction. II. Bond-valence, electrostatic, molecular geometry, and solvation effects. *Geochim. Cosmochim. Acta* **2006**, *70*, 4057–4071.

(18) Ong, S.; Zhao, X.; Eisenthal, K. B. Polarization of water molecules at a charged interface: second harmonic studies of the silica/water interface. *Chem. Phys. Lett.* **1992**, *191*, 327–335.

(19) Macias-Romero, C.; Nahalka, I.; Okur, H. I.; Roke, S. Optical imaging of surface chemistry and dynamics in confinement. *Science* **2017**, *357*, 784–788.

(20) McBriarty, M. E.; von Rudorff, G. F.; Stubbs, J. E.; Eng, P. J.; Blumberger, J.; Rosso, K. M. Dynamic Stabilization of Metal Oxide-Water Interfaces. *J. Am. Chem. Soc.* **2017**, *139*, 2581–2584.

(21) Tanwar, K. S.; Lo, C. S.; Eng, P. J.; Catalano, J. G.; Walko, D. A.; Brown, G. E.; Waychunas, G. A.; Chaka, A. M.; Trainor, T. P. Surface diffraction study of the hydrated hematite $(1\bar{1}02)$ surface. *Surf. Sci.* **2007**, *601*, 460–474.

(22) Hiemstra, T.; Venema, P.; Riemsdijk, W. Intrinsic Proton Affinity of Reactive Surface Groups of Metal (Hydr)oxides: The Bond Valence Principle. *J. Colloid Interface Sci.* **1996**, *184*, 680–692.

(23) Venema, P.; Hiemstra, T.; Weidler, P. G.; van Riemsdijk, W. H. Intrinsic Proton Affinity of Reactive Surface Groups of Metal (Hydr)oxides: Application to Iron (Hydr)oxides. *J. Colloid Interface Sci.* **1998**, *198*, 282–295.

(24) Machesky, M. L.; Wesolowski, D. J.; Palmer, D. A.; Ridley, M. K. On the Temperature Dependence of Intrinsic Surface Protonation Equilibrium Constants: An Extension of the Revised MUSIC Model. *J. Colloid Interface Sci.* **2001**, *239*, 314–327.

(25) Hiemstra, T.; Van Riemsdijk, W.; Bolt, G. Multisite proton adsorption modeling at the solid/solution interface of (hydr)oxides: A new approach: I. Model description and evaluation of intrinsic reaction constants. *J. Colloid Interface Sci.* **1989**, *133*, 91–104.

(26) Hiemstra, T.; De Wit, J.; Van Riemsdijk, W. Multisite proton adsorption modeling at the solid/solution interface of (hydr)oxides: A new approach: II. Application to various important (hydr)oxides. *J. Colloid Interface Sci.* **1989**, *133*, 105–117.

(27) Bickmore, B. R.; Tadanier, C. J.; Rosso, K. M.; Monn, W. D.; Eggett, D. L. Bond-valence methods for pK_a prediction: critical reanalysis and a new approach. *Geochim. Cosmochim. Acta* **2004**, *68*, 2025–2042.

(28) Bickmore, B. R. In *Structure and Bonding*; Brown, I. D., Poeppelmeier, K. R., Eds.; Structure and Bonding September 2005; Springer Berlin Heidelberg: Berlin, Heidelberg, 2013; Vol. 158; pp 191–203.

(29) Brown, I. D.; Altermatt, D. Bond-valence parameters obtained from a systematic analysis of the Inorganic Crystal Structure Database. *Acta Crystallogr., Sect. B: Struct. Sci.* **1985**, *41*, 244–247.

(30) Nsvrotsky, A., Ed. *Structure and Bonding in Crystals*, 1st ed.; Academic Press, 1981.

(31) Cheng, J.; Sprik, M. Acidity of the Aqueous Rutile TiO_2(110) Surface from Density Functional Theory Based Molecular Dynamics. *J. Chem. Theory Comput.* **2010**, *6*, 880–889.

(32) Rustad, J. R.; Felmy, A. R.; Bylaska, E. J. Molecular simulation of the magnetite-water interface. *Geochim. Cosmochim. Acta* **2003**, *67*, 1001–1016.

(33) Rustad, J. R.; Felmy, A. R. The influence of edge sites on the development of surface charge on goethite nanoparticles: A molecular dynamics investigation. *Geochim. Cosmochim. Acta* **2005**, *69*, 1405–1411.

(34) Kerisit, S. Water structure at hematite–water interfaces. *Geochim. Cosmochim. Acta* **2011**, *75*, 2043–2061.

(35) von Rudorff, G. F.; Jakobsen, R.; Rosso, K. M.; Blumberger, J. Fast Interconversion of Hydrogen Bonding at the Hematite (001)–Liquid Water Interface. *J. Phys. Chem. Lett.* **2016**, *7*, 1155–1160.

(36) von Rudorff, G. F.; Jakobsen, R.; Rosso, K. M.; Blumberger, J. Hematite(001)-liquid water interface from hybrid density functional-based molecular dynamics. *J. Phys.: Condens. Matter* **2016**, *28*, 394001.

(37) Van Duin, A. C.; Dasgupta, S.; Lorant, F.; Goddard, W. A. ReaxFF: A Reactive Force Field for Hydrocarbons. *J. Phys. Chem. A* **2001**, *105*, 9396–9409.

(38) Senftle, T. P.; Hong, S.; Islam, M. M.; Kylasa, S. B.; Zheng, Y.; Shin, Y. K.; Junkermeier, C.; Engel-Herbert, R.; Janik, M. J.; Aktulga, H. M.; Verstraelen, T.; Grama, A.; van Duin, A. C. T. The ReaxFF reactive force-field: development, applications and future directions. *npj Comput. Mater.* **2016**, *2*, 15011.

(39) van Duin, A. C. T.; Bryantsev, V. S.; Diallo, M. S.; Goddard, W. A.; Rahaman, O.; Doren, D. J.; Raymand, D.; Hermansson, K. Development and Validation of a ReaxFF Reactive Force Field for Cu Cation/Water Interactions and Copper Metal/Metal Oxide/Metal Hydroxide Condensed Phases. *J. Phys. Chem. A* **2010**, *114*, 9507–9514.

(40) Raymand, D.; van Duin, A. C.; Baudin, M.; Hermansson, K. A reactive force field (ReaxFF) for zinc oxide. *Surf. Sci.* **2008**, *602*, 1020–1031.

(41) Raymand, D.; van Duin, A. C.; Spångberg, D.; Goddard, W. A.; Hermansson, K. Water adsorption on stepped ZnO surfaces from MD simulation. *Surf. Sci.* **2010**, *604*, 741–752.

(42) Raymand, D.; Van Duin, A. C.; Goddard, W. A.; Hermansson, K.; Spångberg, D. Hydroxylation Structure and Proton Transfer Reactivity at the Zinc Oxide–Water Interface. *J. Phys. Chem. C* **2011**, *115*, 8573–8579.

(43) Kim, S. Y.; Kumar, N.; Persson, P.; Sofo, J.; Van Duin, A. C. T.; Kubicki, J. D. Development of a ReaxFF Reactive Force Field for Titanium Dioxide/Water Systems. *Langmuir* **2013**, *29*, 7838–7846.

(44) Raju, M.; Kim, S.-Y.; van Duin, A. C. T.; Fichthorn, K. A. ReaxFF Reactive Force Field Study of the Dissociation of Water on Titania Surfaces. *J. Phys. Chem. C* **2013**, *117*, 10558–10572.

(45) Aryanpour, M.; van Duin, A. C. T.; Kubicki, J. D. Development of a Reactive Force Field for Iron–Oxyhydroxide Systems. *J. Phys. Chem. A* **2010**, *114*, 6298–6307.

(46) Cheng, J.; Sulpizi, M.; Sprik, M. Redox potentials and pK_a for benzoquinone from density functional theory based molecular dynamics. *J. Chem. Phys.* **2009**, *131*, 154504.

(47) Sulpizi, M.; Sprik, M. Acidity constants from DFT-based molecular dynamics simulations. *J. Phys.: Condens. Matter* **2010**, *22*, 284116.

(48) Cheng, J.; Liu, X.; VandeVondele, J.; Sulpizi, M.; Sprik, M. Redox Potentials and Acidity Constants from Density Functional Theory Based Molecular Dynamics. *Acc. Chem. Res.* **2014**, *47*, 3522–3529.

(49) Liu, X.; Cheng, J.; Sprik, M.; Lu, X.; Wang, R. Understanding surface acidity of gibbsite with first principles molecular dynamics simulations. *Geochim. Cosmochim. Acta* **2013**, *120*, 487–495.

(50) Liu, X.; Cheng, J.; Sprik, M.; Lu, X.; Wang, R. Surface acidity of 2:1-type dioctahedral clay

minerals from first principles molecular dynamics simulations. *Geochim. Cosmochim. Acta* **2014**, *140*, 410–417.

(51) Liu, X.; Cheng, J.; Sprik, M.; Lu, X.; Wang, R. Interfacial structures and acidity of edge surfaces of ferruginous smectites. *Geochim. Cosmochim. Acta* **2015**, *168*, 293–301.

(52) Liu, X.; Lu, X.; Cheng, J.; Sprik, M.; Wang, R. Temperature dependence of interfacial structures and acidity of clay edge surfaces. *Geochim. Cosmochim. Acta* **2015**, *160*, 91–99.

(53) Lützenkirchen, J. et al. The surface chemistry of sapphire-c: A literature review and a study on various factors influencing its IEP. *Adv. Colloid Interface Sci.* **2018**, *251*, 1–25.

(54) Mangold, M.; Rolland, L.; Costanzo, F.; Sprik, M.; Sulpizi, M.; Blumberger, J. Absolute pK_a Values and Solvation Structure of Amino Acids from Density Functional Based Molecular Dynamics Simulation. *J. Chem. Theory Comput.* **2011**, *7*, 1951–1961.

(55) Ayala, R.; Sprik, M. A Classical Point Charge Model Study of System Size Dependence of Oxidation and Reorganization Free Energies in Aqueous Solution. *J. Phys. Chem. B* **2008**, *112*, 257–269.

(56) Trainor, T. P.; Eng, P. J.; Robinson, I. K. Calculation of crystal truncation rod structure factors for arbitrary rational surface terminations. *J. Appl. Crystallogr.* **2002**, *35*, 696–701.

(57) CP2K Developers Group. `http://www.cp2k.org`.

(58) VandeVondele, J.; Krack, M.; Mohamed, F.; Parrinello, M.; Chassaing, T.; Hutter, J. Quickstep: Fast and accurate density functional calculations using a mixed Gaussian and plane waves approach. *Comput. Phys. Commun.* **2005**, *167*, 103–128.

(59) Rohrbach, A.; Hafner, J.; Kresse, G. Ab initio study of the (0001) surfaces of hematite and chromia: Influence of strong electronic correlations. *Phys. Rev. B* **2004**, *70*, 125426.

(60) Velev, J.; Bandyopadhyay, A.; Butler, W. H.; Sarker, S. Electronic and magnetic structure of transition-metal-doped α-hematite. *Phys. Rev. B* **2005**, *71*, 1–7.

(61) Grimme, S.; Antony, J.; Ehrlich, S.; Krieg, H. A consistent and accurate ab initio parametrization of density functional dispersion correction (DFT-D) for the 94 elements H-Pu. *J. Chem. Phys.* **2010**, *132*, 154104.

(62) VandeVondele, J.; Hutter, J. Gaussian basis sets for accurate calculations on molecular systems in gas and condensed phases. *J. Chem. Phys.* **2007**, *127*, 114105.

(63) Goedecker, S.; Teter, M.; Hutter, J. Separable dual-space Gaussian pseudopotentials. *Phys. Rev. B* **1996**, *54*, 1703–1710.

(64) Hartwigsen, C.; Goedecker, S.; Hutter, J. Relativistic separable dual-space Gaussian pseudopotentials from H to Rn. *Phys. Rev. B* **1998**, *58*, 3641–3662.

(65) Krack, M. Pseudopotentials for H to Kr optimized for gradient-corrected exchange-correlation functionals. *Theor. Chem. Acc.* **2005**, *114*, 145–152.

(66) VandeVondele, J.; Mohamed, F.; Krack, M.; Hutter, J.; Sprik, M.; Parrinello, M. The influence of temperature and density functional models in ab initio molecular dynamics simulation of liquid water. *J. Chem. Phys.* **2005**, *122*, 014515.

(67) Yang, W.; Bitetti-Putzer, R.; Karplus, M. Free energy simulations: Use of reverse cumulative averaging to determine the equilibrated region and the time required for convergence. *J. Chem. Phys.* **2004**, *120*, 2618–2628.

(68) Flyvbjerg, H.; Petersen, H. G. Error estimates on averages of correlated data. *J. Chem. Phys.* **1989**, *91*, 461–466.

(69) Tanwar, K. S.; Petitto, S. C.; Ghose, S. K.; Eng, P. J.; Trainor, T. P. Fe(II) adsorption on hematite (0001). *Geochim. Cosmochim. Acta* **2009**, *73*, 4346–4365.

(70) Lützenkirchen, J.; Preočanin, T.; Stipić, F.; Heberling, F.; Rosenqvist, J.; Kallay, N. Surface potential at the hematite (001) crystal plane in aqueous environments and the effects of prolonged aging in water. *Geochim. Cosmochim. Acta* **2013**, *120*, 479–486.

(71) Chatman, S.; Zarzycki, P.; Rosso, K. M. Surface potentials of (001), (012), (113) hematite (α-Fe_2O_3) crystal faces in aqueous solution. *Phys. Chem. Chem. Phys.* **2013**, *15*, 13911–13921.

(72) Bargar, J.; Towle, S.; Brown, G.; Parks, G. XAFS and Bond-Valence Determination of the Structures and Compositions of Surface Functional Groups and Pb(II) and Co(II) Sorption Products on Single-Crystal α-Al_2O_3. *J. Colloid Interface Sci.* **1997**, *185*, 473–492.

(73) Catalano, J. G.; Fenter, P.; Park, C. Interfacial water structure on the (012) surface of hematite: Ordering and reactivity in comparison with corundum. *Geochim. Cosmochim. Acta* **2007**, *71*, 5313–5324.

(74) Machesky, M. L.; PrÌŇedota, M.; Wesolowski, D. J.; Vlcek, L.; Cummings, P. T.; Rosenqvist, J.; Ridley, M. K.; Kubicki, J. D.; Bandura, A. V.; Kumar, N.; Sofo, J. O. Surface Protonation at the Rutile (110) Interface: Explicit Incorporation of Solvation Structure within the Refined MUSIC Model Framework. *Langmuir* **2008**, *24*, 12331–12339.

(75) Vlcek, L.; Zhang, Z.; Machesky, M. L.; Fenter, P.; Rosenqvist, J.; Wesolowski, D. J.; Anovitz, L. M.; Predota, M.; Cummings, P. T. Electric Double Layer at Metal Oxide Surfaces: Static Properties of the Cassiterite–Water Interface. *Langmuir* **2007**, *23*, 4925–4937.

(76) Rosenqvist, J.; Machesky, M. L.; Vlcek, L.; Cummings, P. T.; Wesolowski, D. J. Charging Properties of Cassiterite (α-SnO_2) Surfaces in NaCl and RbCl Ionic Media. *Langmuir* **2009**, *25*, 10852–10862.

(77) Eggleston, C. M.; Jordan, G. A new approach to pH of point of zero charge measurement: crystal-face specificity by scanning force microscopy (SFM). *Geochim. Cosmochim. Acta* **1998**, *62*, 1919–1923.

(78) Sung, J.; Zhang, L.; Tian, C.; Waychunas, G. A.; Shen, Y. R. Surface Structure of Protonated R-Sapphire ($1\bar{1}02$) Studied by Sum-Frequency Vibrational Spectroscopy. *J. Am. Chem. Soc.* **2011**, *133*, 3846–3853.

(79) Zhang, L.; Tian, C.; Waychunas, G. A.; Shen, Y. R. Structures and Charging of α-Alumina (0001)/Water Interfaces Studied by Sum-Frequency Vibrational Spectroscopy. *J. Am. Chem. Soc.* **2008**, *130*, 7686–7694.

(80) Chatman, S.; Zarzycki, P.; Preočanin, T.; Rosso, K. Effect of surface site interactions on potentiometric titration of hematite (α-Fe_2O_3) crystal faces. *J. Colloid Interface Sci.* **2013**, *391*, 125–134.